(4)

Final Report

Contract N00014-84-K-0276

FRACTURE MECHANISMS IN IRON AND NICKEL ALUMINIDES

covering the period 1/3/84 - 31/5/88

N.S. Stoloff
Materials Engineering Department
Rensselaer Polytechnic Institute
Troy, NY 12180-3590

August 15, 1988

Unclassified

SECURITY CLASSIFICATION OF THIS PAGE

REPORT DOCUMENTATION PAGE

1a. REPORT SECURITY CLASSIFICATION Unclassified	1b. RESTRICTIVE MARKINGS
2a. SECURITY CLASSIFICATION AUTHORITY	3. DISTRIBUTION/AVAILABILITY OF REPORT ~~Unrestricted~~ DISTRIBUTION STATEMENT A Approved for public release; Distribution Unlimited
2b. DECLASSIFICATION/DOWNGRADING SCHEDULE	
4. PERFORMING ORGANIZATION REPORT NUMBER(S)	5. MONITORING ORGANIZATION REPORT NUMBER(S)
6a. NAME OF PERFORMING ORGANIZATION Rensselaer Polytechnic Institute Materials Engineering Dept 6b. OFFICE SYMBOL (If applicable)	7a. NAME OF MONITORING ORGANIZATION Office of Naval Research
6c. ADDRESS (City, State and ZIP Code) Troy, NY 12180-3590	7b. ADDRESS (City, State and ZIP Code) 800 North Quincy St Arlington, VA 22217
8a. NAME OF FUNDING/SPONSORING ORGANIZATION 8b. OFFICE SYMBOL (If applicable)	9. PROCUREMENT INSTRUMENT IDENTIFICATION NUMBER N00014-84-K-0276
8c. ADDRESS (City, State and ZIP Code)	10. SOURCE OF FUNDING NOS. PROGRAM ELEMENT NO. / PROJECT NO. / TASK NO. / WORK UNIT NO.
11. TITLE (Include Security Classification) Fracture Mechanisms in Iron and Nickel Aluminides	
12. PERSONAL AUTHOR(S) N.S. Stoloff	
13a. TYPE OF REPORT Final 13b. TIME COVERED FROM 84/3/1 TO 88/5/31	14. DATE OF REPORT (Yr., Mo., Day) 88/8/15 15. PAGE COUNT
16. SUPPLEMENTARY NOTATION	
17. COSATI CODES FIELD / GROUP / SUB. GR.	18. SUBJECT TERMS (Continue on reverse if necessary and identify by block number) Intermetallic compounds, aluminides, fatigue, nickel alloys, iron alloys, fracture
19. ABSTRACT (Continue on reverse if necessary and identify by block number) (See Reverse Side)	
20. DISTRIBUTION/AVAILABILITY OF ABSTRACT UNCLASSIFIED/UNLIMITED ☒ SAME AS RPT. ☐ DTIC USERS ☐	21. ABSTRACT SECURITY CLASSIFICATION Unclassified
22a. NAME OF RESPONSIBLE INDIVIDUAL	22b. TELEPHONE NUMBER (Include Area Code) 22c. OFFICE SYMBOL

DD FORM 1473, 83 APR EDITION OF 1 JAN 73 IS OBSOLETE.

Unclassified

SECURITY CLASSIFICATION OF THIS PAGE

ABSTRACT

The high cycle fatigue (HCF) resistance of several boron-doped Ni_3Al alloys has been determined over a range of test temperatures. Fatigue and tensile properties of two Ni-rich ternary alloys were much superior to those of the cast 26%Al alloy or a P/M alloy with 9.3%Mn. Crack paths were transgranular in the Ni-rich alloys and intergranular or interdendritic in Ni-26%Al. HCF lives decreased sharply at temperatures above 500°C. Mn had little effect on this phenomenon. Crack growth rates increased with temperatures to 600°C, in spite of a rising yield stress over the same temperature range, perhaps due to oxygen-induced embrittlement.

Single crystals of Ni_3Al+B displayed a marked flow stress assymetry in tension and compression. A detailed study of fatigue damage (internal and surface) was made. Point defects were observed in large numbers; these condense into voids, thereby contributing to each crack initiation.

The high cycle fatigue (HCF) and crack growth resistance of several Fe_3Al-type alloys was determined in the temperature range 25-600°C. Long range order (DO_3 type) was effective in prolonging high cycle fatigue lives in Fe-28.1%Al, but not in Fe-23.7%Al at 25°C. However, crack growth rates were higher in the DO_3 condition. The fatigue resistance of DO_3 material was not as severely affected by test temperature as was that of B2 material. A substantial creep component was noted in both HCF and crack growth tests on B2 material at 560°C and 600°C. Fracture surfaces consisted primarily of cleavage facets in all alloys and conditions of order, but crack initiation was intergranular in Fe-Al tested in HCF. Cracks initiated transgranularly in pre-notched crack growth samples. Fatigue striations were observed only at 500°C in both types of tests.

Fatigue results on both Ni_3Al and Fe_3Al alloys are discussed on the basis of microstructure, surface slip band development and internal dislocation substructures revealed by transmission electron microscopy.

ABSTRACT

The high cycle fatigue (HCF) resistance of several boron-doped Ni_3Al alloys has been determined over a range of test temperatures. Fatigue and tensile properties of two Ni-rich ternary alloys were much superior to those of the cast 26%Al alloy or a P/M alloy with 9.3%Mn. Crack paths were transgranular in the Ni-rich alloys and intergranular or interdendritic in Ni-26%Al. HCF lives decreased sharply at temperatures above 500°C; Mn had little effect on this phenomenon. Crack growth rates increased with temperatures to 600°C, in spite of a rising yield stress over the same temperature range, perhaps due to oxygen-induced embrittlement.

Single crystals of Ni_3Al+B displayed a marked flow stress assymetry in tension and compression. A detailed study of fatigue damage (internal and surface) was made. Point defects were observed in large numbers; these condense into microvoids, thereby contributing to easy crack initiation.

The high cycle fatigue (HCF) and crack growth resistance of several Fe_3Al-type alloys was determined in the temperature range 25-600°C. Long range order (DO_3 type) was effective in prolonging high cycle fatigue lives in Fe-28.1%Al, but not in Fe-23.7%Al at 25°C. However, crack growth rates were higher in the DO_3 condition. The fatigue resistance of DO_3 material was not as severely affected by test temperature as was that of B2 material. A substantial creep

component was noted in both HCF and crack growth tests on B2 material at 560°C and 600°C. Fracture surfaces consisted primarily of cleavage facets in all alloys and conditions of order, but crack initiation was intergranular in Fe-Al tested in HCF. Cracks initiated transgranularly in pre-notched crack growth samples. Fatigue striations were observed only at 500°C in both types of tests.

Fatigue results on both Ni_3Al and Fe_3Al alloys are discussed on the basis of microstructure, surface slip band development and internal dislocation substructures revealed by transmission electron microscopy.

I. INTRODUCTION

Intermetallic compounds such as Ni_3Al and Fe_3Al offer potential advantages of low density, high strength and good oxidation resistance. However, attempts to develop these alloys have been hindered by their brittleness and notch sensitivity at low temperatures[1-3]. Recently, modest improvements in ductility have been achieved in Fe-Al alloys through the preparation of pure, relatively fine-grained alloys[4-5]. In the case of Ni_3Al, boron in small quantities provides a striking increase in room temperature ductility for alloys in which Al<24a%[6-8].

Little is known about fatigue behavior of polycrystalline nickel and iron aluminides. The present work represents an account of the response of polycrystalline Ni_3Al and Fe_3Al to stress-controlled cyclic loading between 25°C and 800°C. Both high cycle fatigue (HCF) experiments on unnotched bars, and crack growth (da/dN) studies on compact tension samples were carried out. Experimental variables were aluminum content and manganese content for Ni_3Al and aluminum content and type of long range order (DO_3 vs partial B2) for Fe_3Al. In alloys near Fe-25%Al, DO_3 order occurs at a critical temperature of about 550°C. Quenching from above that temperature results in the formation of partial B2 type order. Phase relationships in this system are still not well established, as Inoue[9] has shown that two phase α+B2 and α+DO_3 regions can exist near Tc, the critical ordering temperature of alloys with less than 26%Al. In addition to the work on polycrystals, strain controlled experiments have been carried out on Ni_3Al+B single crystals, oriented for single slip. These experiments were aimed at determining the type and rate of

accumulation of surface and internal damage resulting from cyclic loading, and to relate this damage to the formation of cracks.

II. ALLOYS AND EXPERIMENTAL PROCEDURE

A - Ni_3Al

Alloys for tensile and high cycle fatigue tests were obtained from various sources. An argon drop cast ingot of Ni-26a%Al-0.25%B was provided by D.M. Shah of Pratt & Whitney Aircraft. Another drop cast ingot, containing 23.4a%Al-0.5%Hf-0.26%B (designated IC-50) was provided by C.T. Liu of Oak Ridge National Laboratory; sheet materials of the same alloy also was provided. Powder of composition Ni-24%Al-1.2%Fe-0.25%B was provided by Dr. S.C. Huang of General Electric Co. Corporate Research and Development Center; powder of composition Ni-15.23a%Al-9.36%Mn-0.2%B was obtained from Special Metals Corp. Both alloys were hot isostatically pressed (HIP) under conditions of 1150°C, 103MPa for 2 hrs. Samples were electro-discharge machined (EDM) from the drop cast ingot and the HIP can. In addition HIP material was extruded at 1100°C with a 7:1 reduction. Final specimens for tensile and high cycle fatigue tests had a cylindrical gage section 12.1 mm long with a 2.54 mm diameter. The HIP + extruded samples were heat treated in flowing hydrogen at 1000°C for three hours and furnace cooled, while the As-HIP and drop cast samples were annealed at 1000°C for 1 hour. This produced similar grain size (30-40 μm) in the HIP alloys, while Al-rich alloy had an 80 μm grain size. IC-50 had a grain size of 48 μm after that heat treatment at 1000°C for one hour, followed by a furnace cool.

Single crystals of Ni-24a%Al-0.25%B was obtained from Pratt and Whitney Aircraft Div, United Technologies Corp. Test samples were prepared in the form of 3x3x9 mm gage sections prepared by electro-discharged machining. Most crystals were oriented near [$\bar{2}$ 13 17]. All samples were annealed in vacuum for 50 hrs, and electropolished prior to testing under strain control conditions at a strain rate of 5×10^{-4} 5^{-1}.

After abrasive polishing and electropolishing (10% perchloric acid in glacial acetic acid at 5°C), the polycrystalline samples were tested in an Instron closed loop machine either in stress-controlled fatigue or stroke-controlled tensile tests. Room temperature tests were carried out in air, while elevated temperature tests were performed in vacuum of 1.36×10^{-3}Pa ($1x10^{-5}$) torr or better. Tensile tests were run at a strain rate of $3.3x10^{4}s^{-1}$ while fatigue tests were performed with a triangular wave function at a frequency of 20 Hz with $R = \sigma_{min}/\sigma_{max} = 0.1$. After testing, each sample was examined in the scanning electron microscope (SEM). Limited transmission electron microscopy (TEM) observations were carried out on foils polished with 10% perchloric acid, 45% glacial acetic acid and 45% monobutyl ether, at 5°C.

Crack propagation experiments were conducted on compact tension type specimens with W=25.4mm and B=2.16mm, machined from rolled plates of IC-50. The experiments were conducted at a frequency of 20 Hz and an R-ratio of 0.1, in a vacuum of 1.36×10^{-3}Pa ($1x10^{-5}$ torr) or better. Crack growth measurements were made using an optical microscope to observe one specimen surface.

B - Fe_3Al

Alloys were supplied by Olin Corp, General Electric Co. and Oak Ridge National Lab. Compositions and grain sizes are listed in Table 1. Before testing, specimens were heat treated to produce B2 or DO_3 type superlattices as follows:

B2 : 850°C/1h/quench in iced water

DO_3 : B2+325/1h/furnace cool

Three types of tests were conducted : tensile and high cycle fatigue tests on cylindrical rod, and crack growth experiments on specimens cut from plate. Tensile and high cycle fatigue samples had gage length 12.5 mm long x 2.54 mm dia. Some tensile bars had a V-notch. Tensile tests were conducted on a screw-driven Instron machine at a strain rate of $3.3 \times 10^{-4} s^{-1}$. High cycle tests were performed in air in stress control with $R = \sigma_{min}/\sigma_{max} = 0.1$. Compact tension samples approximately 30 mm square were employed for crack growth tests. Friction grips were used, since pin loading caused specimen failure through the loading pin hole. Specimens were cycled in air at a frequency of 20 Hz with R = 0.1. Crack growth rate was measured at room temperature by a traveling microscope. The DC potential drop method was used to measure the crack growth rate at elevated temperatures.

III. EXPERIMENTAL RESULTS

A - Ni_3Al

1. Tensile Behavior

Tensile properties for the various test materials are listed in Table 2. The HIP + extruded 24%Al alloy exhibited yield and ultimate tensile strengths superior to that of the as-HIP alloy at room temperature and 500°C. The HIP + extruded alloy displayed significant notch

sensitivity; it is presumed that all boron-doped binary alloys would be extremely notch sensitive. The two binary alloys had similar ductility at room temperature but at 500°C the as-HIP alloy exhibited decreased ductility while the HIP + extruded alloy increased slight in ductility. However, both 24% Al alloys were much more ductile than the 26%Al alloy, which displayed only 5% elongation at 25°C and no ductility at 500°C. Data for IC-50 were taken from the literature[7]. The effect of 0.5% Hf is to increase the yield strength of Ni_3Al+B from 240MPa to 310MPa. The ductility of this alloy is higher than that of any of the PM alloys.

The Mn-containing alloy showed reduced strength and ductility at all test temperatures compared to identically processed Ni_3Al+B, compare Figs. 1a) and b), probably because of a higher volume fraction of pores in the former. However, tests on notched bars showed that Mn eliminated the notch sensitivity of Ni_3Al+B at both 25°C and 500°C, see Table 2.

Tensile tests on unnotched bars of Fe_3Al revealed very low ductilities at room temperature; ductility was reduced to zero in the presence of a notch, see Table 3. The notch sensitivity ratio (notched/unnotched tensile strength) was 0.57 for DO_3 order and 0.79 for B2 order, demonstrating the greater notch sensitivity of the DO_3 condition.

2. High Cycle Fatigue

The HIP + extruded 24%Al alloy was superior to both the as-HIP 24%Al and the cast 26%Al alloys at all stress levels at room temperature in high cycle fatigue (Fig. 2a). The differences between the two HIP alloys were magnified by normalizing the data (dividing the stress amplitude by the respective yield stress), see Fig. 2b). Note that

absolute and normalized fatigue data for HIP Ni_3Al fall on the same curve as previously obtained data for cast, wrought and recrystallized IC-50[10]. The Mn-containing alloy showed inferior fatigue resistance at both 25°C and 500°C, as shown in Fig. 3a) and 3b) respectively.

Fatigue cracks initiated at defects (pores or inclusions) at the sample surface at about 50% of the life for all P/M alloys. The crack grows in a stage I mode, until it reached some critical length at which overload occurs; the latter region revealed intergranular facets for Ni-24Al+B, but transgranular cracking was observed in the alloy with 9.3Mn.

In IC-50, on the other hand, cracks always initiated in a stage I mode along slip bands, and continued to propagate transgranularly until overload occurred. Again the overload region displayed intergranular facets. For Ni-26%Al, cracks generally initiated and propagated intergranularly or interdendritically.

The HIP + extruded alloy exhibited no significant change in fatigue life between 25°C and 500°C, except perhaps at very low stress levels, see Fig. 4. The as-cast 26%Al alloy actually was more fatigue resistant at 500°C than at 25°C at all stress levels. However, the higher Al content and load structure resulted in poor fatigue resistance relative to the 24%Al alloy at both temperatures. The reason for this is quite clear in that the tensile strength of Ni-26a%Al is much lower than for Ni-24a%Al at both 25°C and 500°C, see Table 2; further, the 26%Al alloy exhibits only slight ductility at 25°C and none at 500°C, so that once a crack is nucleated, rapid propagation is inevitable.

When the data for Ni-24a%Al were normalized for strength differences, room temperature lives were greater than high temperature lives.

Cracks initiated internally at defects near the surface in HIP or HIP + extruded material. In the 24%Al alloy the cracks propagated transgranularly and then overload occurred in a totally intergranular mode. The 26%Al alloy again failed intergranularly or interdendritically at 500°C.

In addition to the tests at 500°C, fatigue tests were run on HIP + extruded Ni-24%Al at 600°C, 700°C and 800°C in vacuum, at a stress range of 500MPa. The life vs temperature curve somewhat resembled the anomolous yield strength behavior of Ni_3Al, with a shallow peak at 500°C and a rapid drop off above 600°C (Fig. 5a). Fracture was intergranular at all temperatures above 500°C. Similar behavior was noted in the Mn-containing alloy, Fig. 5b).

3. Crack Growth

Crack growth experiments were carried out on Ni_3Al+B+Hf (IC-50) at 25°C, see results in Fig. 6. Also shown are data for commercial alloys as well as two long range ordered alloys, LRO-42 and LRO-60, tested under similar conditions in our laboratory[11]. Note that the LRO alloys and IC-50 display a decided advantage over the commercial alloys, especially at low ΔK.

The rate of crack growth in IC-50 increases with temperature (although there is little difference between 500°C and 600°C), see Fig. 7. At 500°C crack growth rates are about 100 times higher than at 25°C, although the data of Table 2 for HIP + extruded Ni-24%Al show decreased notch sensitivity at the higher temperature.

Stage I (slip-band) cracking was noted at room temperature, see Fig. 8; the tendency for stage I cracking was reduced with increasing temperature. At temperatures near 600°C, Fig. 9, Ni_3Al+B displays

a higher crack growth rate than LRO-60, but generally cracks at a lower rate than commercial alloys at $\Delta K<20$ MPam$^{-1/2}$. Data for LRO-60[11], René 95[12] and Astroloy[12] were determined in our laboratory under identical cycling conditions, but in argon.

4. TEM Observations

Limited TEM observations at magnifications to 290,000 times failed to reveal any separation of pairs of unit dislocations in any of the polycrystalline Ni_3Al alloys tested. Planar arrays of dislocation were observed in all of the alloys, but especially so in the Ni-26%Al alloy. No tendency for cell structure formation was noted for specimens tested at any temperature to 800°C.

5. Single Crystals

Single crystals of Ni_3Al, oriented as shown in Fig. 10, have been tested in both tension and fatigue at 25°C in air. Note the flow stress assymetry between tension and compression. Tensile tests have shown that several {111} systems are operative. Cycled samples also have been examined to observe the development of surface slip traces, as in Fig. 11a) and b). Persistent slip bands have been seen at 50 cycles into the test, as can be noted clearly in Fig. 11a). Their development into cracks can be seen in Fig. 11b). At high magnification in the SEM the development of extrusions and intrusions into cracks is clearly evident, as shown in Fig. 12a). These cracks usually consist of segments on two or more planes. Fracture facets on cube planes have been identified.

The development of PSBs is accompanied by the formation of small voids, as shown in Fig. 12b). The accumulation of vacancies during fatigue appears to lead to the nucleation and growth of vacancy loops,

as noted by TEM, Fig. 13 and 14. These loops, many of which are faulted, may coalesce into the voids shown in Fig. 12b). In most cases long, straight screw dislocations are seen, on up to three systems. The antiphase boundary energy on {111} has been calculated from weak beam experiments to be about $140 mJ/m^2$, in agreement with published data[29].

B - Fe_3Al

1. High Cycle Fatigue

The results of high cycle fatigue (HCF) tests as a function of composition and temperature are shown in Figs. 15-17. Fig. 15 shows that at room temperature HCF resistance in Fe-23.7%Al is independent of the type of order except at the lowest stress level, where the B2 condition demonstrated higher fatigue resistance. Also shown in Fig. 15 is a relatively strong dependence of HCF life on temperature for the B2 condition, with only a small effect for DO_3 samples between 25°C and 500°C.

For Fe-28.7a%Al, the DO_3 condition is superior to B2 material at 25°C, Fig. 16. However, this alloy is sensitive to temperature in both B2 and DO_3 conditions.

Fig. 17 shows that at 600°C composition has a very strong influence on HCF life. At Δ=200MPa there is about a ten fold increase in life as Al increases from 23.7 to 28.7%. Also shown in Fig. 17 is the steep decrease in life for Fe-23.7%Al between 560°C and 600°C.

Crack initiation at 25°C and 500°C always occurred at grain boundaries, as shown in Fig. 18a). Propagation quickly changed to a predominantly transcrystalline, cleavage-like path, although some intergranular facets would be seen, Fig. 18b). At 500°C only the switch to a transgranular path was accompanied by the formation of

fatigue striations, Fig. 19a). The striations are superimposed upon cleavage markings, Fig. 19b). The fractographic features for DO_3 and B2 material were similar to 500°C. However, tests above Tc caused extensive plastic deformation and necking, consistent with the short fatigue lives previously noted (Fig. 17).

2. Crack Growth

At 25°C, the crack growth rate for Fe-24.93%Al and Fe-25.05%Al was higher in the DO_3 than in the B2 condition, see Fig. 20. Little effect of increasing Al content to 28.4% was noted for the DO_3 material at 25°C.

SEM fractographic analysis showed very little localized plastic deformation at room temperature. Crack propagation was by transgranular cleavage. No evidence of striation formation was noted. Also the fatigue crack started transgranularly at the machined notch.

The crack growth rate at 500°C (DO_3 structure) is higher than that at room temperature at $\Delta K < 31 MPa \sqrt{m}$. At higher ΔK, a cross-over was observed such that the crack growth rate was lower at 500°C than at room temperature. This cross-over roughly corresponds to the onset of the striation markings on the fracture surface.

The fracture appearance at 500°C is similar to that of samples tested at room temperature below $\Delta K = 31 MPa \sqrt{m}$, but above $\Delta K = 31 MPa \sqrt{m}$ striations on the cleavage fracture plane was observed. Dimples were observed in the overload zone.

The crack growth rate at 600°C (B2 structure) is much higher than at room temperature and 500°C. However, the fracture mode remained transgranular cleavage. Some striation markings were noted at high

ΔK. Extensive necking was observed at 600°C, in agreement with the HCF results.

The crack growth rates at elevated temperatures converge to those of room temperature beyond $\Delta K = 40 MPa \sqrt{m}$.

Slopes of the Paris-Erdogan[13] relation are listed in Table 4. There is a sharp drop in slope with increasing test temperature. Transmission electron microscopy revealed that for Al contents of 25.05% or more, dislocations were paired in cycled Fe_3Al, while for 23.7%Al dislocations were unpaired. Generally, at room temperature dislocations were observed only in limited regions of the thin foil. However, at high temperatures, dislocations were found uniformly through the material. A summary of observations on dislocation pairing appears in Table 5. Screw dislocations were usually observed. The distance between pairs is 170Å, which is close to the calculated spacing[14].

IV. DISCUSSION

A - Ni_3Al

1. High Cycle Fatigue

The limited number of alloys tested and the different processing techniques impede rigorous discussion of the results. However, certain broad trends of behavior have emerged from this work:

1) High cycle fatigue resistance of as-HIP and cast and wrought Ni-rich Ni_3Al+B alloys is very similar at 25°C (Fig. 2).

2) Increasing temperature to 500°C does not diminish high cycle fatigue resistance of Ni-rich material (Fig. 4), and actually leads to an increase in life for Ni-26%Al+B.

3) Fatigue resistance drops sharply as Al content is raised from 24 to 26%Al (Fig. 2) or temperature is raised above 500°C (Fig. 5a). Mn has little effect upon this drop in life, Fig. 5b).

4) Ni-24%Al+B is ductile in the unnotched condition, but is highly notch sensitive at 25°C; notch sensitivity is diminished at 500°C, or by the addition of Mn, see Table 2.

5) Ni-26%Al+B is brittle even in the unnotched condition, at both 25°C and 500°C, (Table 2).

The poor behavior of the Ni-26%Al alloy appears to be directly related to the poor ductility and tendency for intergranular fracture in Al-rich Ni_3Al. Further contributing to the low fatigue resistance is the coarse grained cast structure, which is not appreciably altered by the annealing treatment prior to test. We shall confine the balance of the discussion to Ni-rich alloys.

A comparison of the variation of high cycle fatigue life with temperature (Fig. 5) and the variation of crack growth rate with temperature (Fig. 7) suggests that there is enhanced resistance of polycrystalline Ni_3Al to crack initiation with temperature up to about 500°C. At 500°C, for example, while fatigue life is not significantly different from that at room temperature (except perhaps at low stress levels) the rate of crack propagation is increased considerably. The rapid decrease in high cycle life noted at $\Delta\sigma$=500MPa (Fig. 7) almost certainly is due to an environmental effect, since the tensile strength above 500°C also drops sharply[15].

B - Crack Propagation

As shown in Fig. 7 , the rate of crack propagation in Ni_3Al+B+Hf increases rapidly between 25°C and 500°C, with a further small increase in rate at 600°C. (The relatively minor addition of hafnium, though

affecting the strength, is not expected to alter the fatigue crack initiation and propagation mechanisms in polycrystalline Ni_3Al.) At a stress intensity factor of about 30MPam$^{\frac{1}{2}}$, an increase in temperature to 500°C results in an increase in the rate of crack propagation by about two orders of magnitude.

The behavior of Ni_3Al+B+Hf is consistent with previous work[11,16] on crack growth in an $(Fe,Ni)_3V$ alloy. Both types of alloy reveal a higher threshold stress intensity at which fatigue cracks start to grow, compared to superalloys. Chang et al[17] have confirmed this observation on P/M Ni_3Al+B alloys tested at 400°C. However, they also report a higher stage II growth rate than superalloys, when tests are conducted in air, and attributed this behavior to an environmental effect.

We have previously shown that $(Fe,Ni)_3V$ displays an increase in the rate of crack propagation with increasing temperature[16]. This increase in rate also occurs simultaneously with a rising yield stress with temperature, and was attributed to either i) an environmental effect which becomes more pronounced with increasing temperatures, ii) localized disordering at the crack tip due to accumulation of fatigue damage, iii) reduced work hardening with increasing temperature, or some combination of these factors. However, it should be noted that the $(Fe,Ni)_3V$ alloy also showed improved resistance to crack propagation in the ordered condition as compared to the disordered condition at room temperature[16]. This improvement, especially near threshold stress intensity values, was explained on the basis of the unique dislocation dynamics in the ordered lattice; that is, superlattice dislocation must be emitted at a crack tip in the ordered condition in order for crack advance to occur. For example, one

may use the model of McClintock quoted by Tschegg and Stanzl[17] to relate to the Burgers vector, of dislocations emitted at the crack tip to the minimum crack tip opening displacement, $\delta = \frac{\Delta K^2}{E\sigma_{ys}}$. For tension-tension loading, $R \tilde{=} 0$ and $K_{max} \tilde{=} \Delta K$. Therefore:

$$\delta_{min} \tilde{=} b \tilde{=} \frac{\Delta K^2}{E\sigma_{ys}} Th \qquad (1)$$

Solving for ΔK_{Th}, one obtains the following relation

$$\Delta K_{Th} \tilde{=} \sqrt{E\sigma_{ys} b} \qquad (2)$$

The influence of long range order on modulus, E, and yield stress σ_{ys}, cannot be measured in Ni_3Al, which is ordered to the melting point. However, on this simple model, the pairing of dislocations in an ordered lattice (b→2b) should result in about a 40% increase in ΔK_{Th}. This is about the magnitude of increase in apparent ΔK_{Th} in $(Fe,Ni)_3V$[11,16], where σ_{ys} is known to be little affected by order and changes in E also should be small.

Unfortunately, the observed increase in crack growth rate with temperature for Ni_3Al is not consistent with the above, since σ_{ys} increases substantially between 25°C and 500°C, Table I. The anomalous strengthening with temperature observed in $L1_2$ alloys has been discussed in considerable detail[9,18-20]. The essence of most models is the increased tendency for cross slip of the leading dislocation of a superlattice dislocation due to an increase in temperature, thus permitting the antiphase boundary to attain a minimum energy configuration on a {100} plane. However, there is considerable dispute in the literature over this question, with reports both supporting and denying a lowering of energy on {100}. Paidar et al[22] have suggested that the ratio $\gamma_{111}/\gamma_{100}$ must be at least $\sqrt{3}$ for superlattice dislocation

cross slip to occur. The result of a cross slip event is that further movement of this superdislocation is impeded and sessile dislocation segments are created, thus contributing to an increase in the yield strength with temperature.

Let us now consider the three possible hypotheses mentioned above as pertaining to temperature effects on crack growth:

The crack propagation experiments on Ni_3Al+B at elevated temperatures were conducted in moderate vacuum. Although this does not preclude any detrimental interaction between oxygen and the material, the surface appeared shiny after the test. Further, the vacuum used in these tests supressed intergranular fracture and reduced the magnitude of the tensile ductility minimum observed in polycrystalline Ni_3Al tested at elevated temperatures in air[15,23]. Nevertheless, an environmental effect cannot be ruled out in explaining the increased crack growth rates at high temperatures.

Regarding localized disordering, the $(Fe,Ni)_3V$ alloy had an order-disorder transformation temperature of about 720°C and, therefore, stress-assisted disordering was a possibility. However, Ni_3Al remains ordered up to the melting point and would be expected to disply minimal disordering due to accumulation of fatigue damage, even at elevated temperatures. Although work hardening could be expected to decrease with temperature (based on the decrease of UTS with temperature), this factor alone would not explain the observed behavior because the effect of temperature on ease of crack initiation should be similar, but appears in fact, to be different. At all temperatures fatigue cracking initially was crystallographic, i.e., along slip bands. The stage I cracking is indicative of the planar nature of slip in

the initial stages of crack propagation and the relatively low levels of cross slip. With increase in temperature, the relative amount of slip band cracking decreases; the overload region in all the doped binary specimens was completely intergranular.

Whether an existing crack can grow or not under cyclic conditions will depend on the stress accommodative mechanisms available at the crack tip. At any given stress level, stress accommodation is increased by an increase in temperature up to the point where the strains involved reach the available ductility at the crack tip. At the stress intensities employed in these tests, the localized strain at the crack tip is, by definition, large enough to continue the cracking process with further cycling.

This reasoning and the application of Eq. 2 implies that the threshold stress intensity (strictly defined as that value below which a crack does not grow) in Ni_3Al should increase with temperature up to about 500°C, corresponding to high cycle fatigue observations. The data of Fig. 7 do not support such a trend, but the experimental procedures used in this study were not conducive to measuring extremely low rates of crack propagation, near the "true" threshold. Therefore, further work is needed to examine the temperature dependence of near-threshold behavior. It is important to note, however, that in spite of increasing crack growth rates with temperature, Ni_3Al+B remains superior to commercial superalloys at low ΔK levels, as was shown in Figs. 7 and 9.

C - Single Crystals

Previous investigations of cyclic hardening in ordered alloys have been sparse. Chien and Starke[24] noted more rapid cyclic hardening

in the ordered condition for Cu_3Au. However, cyclic strain softening quickly occurred in ordered material only. The small asymmetry in peak stress noted for ordered Cu_3Au was confirmed in our own work on the isomorphous Ni_3Al crystals, Fig. 10. Another similarity noted between Cu_3Au and Ni_3Al is the observation of slip on the primary, (111) $[\bar{1}01]$ system early in the fatigue test, which for Cu_3Au was followed by the formation of deformation bands. Unlike Cu_3Au, where cracks were nucleated at the intersection of slip bands and deformation bands near the grips, cracks in Ni_3Al developed along primary (111), secondary $(\bar{1}11)$ and cross slip $(1\bar{1}1)$ bands, as is clearly visible in Figs. 11 and 12. Chien and Starke could not account for the extensive deformation band cracking in Cu_3Au, although they suggested that extrusion-intrusion progress is exaggerated at the intersection of slip and deformation bands. However, no extrusions or intrusions were shown in that work.

Our results are generally consistent with observations recently reported by Bonda, et al[25,26] for $Ni_3(Al,Nb)$ single crystals, but are much more detailed in the analysis of damage induced by cyclic loading. Flow stress asymmetry was found to be orientation dependent in that work, with strengthening more rapid in compression than in tension over most of the stereographic triangle. A small density of edge dislocation dipoles and many screw dislocations were found at room temperature. However, no vacancy loops or voids were observed in conjunction with slip band cracks[25].

Our observations of faulted loops and other evidence for an apparent excess of vacancies formed under cyclic loading, Figs. 13 and 14, are in general agreement with a model of crack initiation

which postulates that high plastic strain amplitudes lead to the formation of non-equilibrium point defects in PSBs[27]. The defects are distributed inhomogeneously; their migration over short distances causes mass transport, resulting in extrusion and intrusion formation. A kinetic model of crack initiation at PSBS is being developed to explain our experimental observations.

2. Fe_3Al

A. Tension

The tensile ductility of Fe-23.7%Al is very low at room temperature, in contrast to recent reports of 5-7% ducility[4,5]. This difference is attributable more to grain size differences than to impurity content, carbon being known to reduce ductility sharply. The coarse grain size of the sheet alloys, noteably Fe-21.9%Al, Table 1, accounts for both low ductility and relatively low strength of this alloy. High notch sensitivity is not unexpected in these alloys; however, the higher value of notch sensitivity ratio associated with partial B2 order than with complete DO_3 order cannot be explained.

B. High Cycle Fatigue

The high cycle fatigue results show no substantial effect of the type and degree of order on Fe-23.7%Al tested at room temperature. However Fe-28.7%Al is clearly superior in HCF resistance at 25°C relative to B2 material. This may be attributable to dislocation pairing in the DO_3 condition of this alloy, which does not occur in alloys with less than 25%Al. Test temperature has a very substantial influence on HCF life of B2 material, Figs. 15 and 17, undoubtedly due to a strong creep-fatigue interaction at temperatures above 500°C.

DO_3 Fe-23.7%Al, which could only be tested below Tc (550°C) showed little loss in life from 25°C to 500°C, while Fe-28.7% showed a sharp drop in life in the same temperature range. The reason for this difference in behavior with Al content is not known.

The lack of a significant effect of higher Al content on HCF life at 560-600°C seen in Figs. 15 and 16 is surprising unless one takes into account recent information on phase relationships in the Fe-Al system. Inoue has recently published a revised portions of the Fe-Al phase diagram in the range 21-29%Al, see Fig. 21[9]. We have confirmed the two-phase microstructure in Fe-rich Fe_3Al, see Fig. 22. Therefore the fatigue test results are consistent with a picture of an age hardening contribution to life in Fe-23.7%Al at 500°C but not at room temperature, see Fig. 23. The data in Fig. 24, replotted from Figs. 16 and 17, show that Fe-28.7%Al is more fatigue resistant than Fe-23.7%Al at 25°C, but the reverse is observed at 500°C. The existence of an anomalous two-phase hardening contribution to Fe-23.7%Al can explain this reversal.

The HCF behavior at room and elevated temperatures is noteworthy for the highly faceted fracture surfaces that result. Initiation occurs at near-surface grain boundaries but subsequent propagation is by what appears to be rapid cleavage cracking. At temperatures of 500°C and above striations are noted superimposed on the cleavage fracture surfaces (e.g., Fig. 19) suggesting that the total crack growth rate is made up of a combination of static (cleavage) and dynamic (crack blunting) modes.

C. Crack Growth

The crack growth results shown in Fig. 20 are compared to those for other imtermetallics (Ni_3Al+B and Fe,Ni_3V) and for several solid

solution commercial alloys tested at room temperature under comparable conditions. Crack growth is more rapid in Fe-Al alloys than in the other intermetallics, especially at high ΔK. The relatively low ordering energy in Fe_3Al (DO_3), the partial B2 order present in quenched Fe_3Al, and the contribution of cleavage cracking to fatigue crack growth are possible reasons for the higher growth rates in Fe_3Al. Further, the very rapid crack growth and short HCF lives of Fe-25.0%Al at 500°C and 600°C appears to be due to a substantial creep contribution in the tension-tension loading cycle, as manifested in distinct necking of the samples. At 600°C, cleavage and striated growth still occurred in this alloy, in spite of pronounced necking prior to fracture.

The paired dislocations observed in alloys containing at least 25%Al confirms a previous report of Morgand et al[28] that superlattice dislocations are not seen in hypostoichiometric material. Since the presence of superlattice dislocations should affect crack initiation it is not surprising that significant compositional effects have been found in this study; for example HCF lives of Fe-28.7%Al are much higher than for Fe-23.7%Al in the DO_3 condition at 25°C. However, little effect of composition on crack growth has been observed, see Fig. 20.

V. SUMMARY AND CONCLUSIONS

The high cycle fatigue behavior of Ni_3Al+B has been shown to depend upon aluminum and manganese content and processing history; increasing Al content to 26% is very detrimental to high cycle fatigue life, especially at high stress levels. Ni-24a%Al+B made from powder shows little dependence of fatigue life on temperatures between 25°C and 500°C, except perhaps at very low stress levels. Crack growth, on the other hand, is more rapid with increasing temperature, as

measured in a hypostoichiometric alloy containing 0.5%Hf. The high cycle fatigue resistance is sharply reduced and the crack path changes from intergranular to transgranular for Ni-25%Al relative to Ni-24%Al. Although the cast structure of the 26%Al alloy undoubtedly contributes to poor fatigue life, the major effect is probably due to the hyper-stoichiometric Al content, as in tension experiments. Manganese decreases strength and fatigue life of Ni_3Al+B, primarily due to increased porosity. The primary effect of manganese is to reduce both sensitivity of Ni_3Al+B.

Crack growth thresholds in alloy IC-50 (as in other ductile ordered alloys) are higher than in conventional alloys, perhaps due to difficulty in nucleating dislocation pairs at a crack tip. Crack growth rates incease with temperature between 25°C and 600°C, in spite of a rising yield stress and decreasing notch sensitivity over the same temperature range. Environmental effects at elevated temperatures are significant at high stress levels, as noted in HCF tests, and may influence crack growth rates as well.

The HCF and crack growth behavior of Fe_3Al-type alloys is affected by both composition and type and degree of long range order. DO_3 order is effective at room temperature in prolonging HCF life in a hyperstoichiometric alloy, probably due to paired (superlattice) dislocations delaying crack initiation. At elevated temperature it is likely that a two phase microstructure in Fe-23.7%Al accounts for its unusually high fatigue resistance relative to Fe-28.7%Al.

Crack growth is more rapid in Fe_3Al than in ductile Ni_3Al and LRO alloys, probably due to the lower ordering energy and the superposition of cleavage cracking on cycle modes of crack advance in Fe_3Al.

7) G.E. Fuchs and N.S. Stoloff "High Cycle Fatigue of Polycrystalline Ni_3Al and $Ni_3(Al,Mn)$, Proc. Eigth Int Conf on Strength of Metals and Alloys, Tampere, Finland, Aug 22-26, 1988, in press.

8) L.M. Hsiung and N.S. Stoloff "Cyclic Hardening and Crack Initiation in Intermetallic Compounds", Proc Eigth Int Conf on Strength of Metals and Alloys, Tampere, Finland, Aug 22-26, 1988, in press.

In addition, G.E. Fuchs has completed his ONR-supported PhD thesis "The Effects of Order, Temperature and Stoichiometry on the Tensile and High Cycle Fatigue Behavior of Intermetallic Compounds".

Several invited seminars arising from this work have been presented at the University of Birmingham, Oxford Univ., Cambridge Univ. and Berkeley Nuclear Labs in England, at the Ecole Polytechnic Federale de Lausanne in Switzerland and at the Max Planck Institute fur Metallforschung in Dusseldorf, W. Germany and at the Korea Advanced Institute of Science and Technology, Seoul, Korea. Invited papers have been presented at the European Conf. on Applied Physics, Berlin and at the Materials Reseach Society Symposia on High Temperature Ordered Intermetallic Alloys in Boston in Dec. 1984 and Dec.1986.

ACKNOWLEDGMENT

The author is grateful to the US Office of Naval Research for financial support under Contract No. N00014-84-K-0276.

REFERENCES

1. W. Justusson, V.F. Zackay and E.R. Morgan, Trans. ASM, V. 49, p. 905 (1957).
2. M.J. Marcinkowski, M.E. Taylor and F.X. Kayser, J. Mat Sci., V. 10, p. 406 (1975).
3. T. Takasugi and O. Izumi, Acta Met. V. 33, p. 1247 (1985).
4. S.K. Ehlers and M.G. Mendiratta, Abstract, J. of Metals. V. 33 (12), p. 5 (1981).
5. D.K. Chaterjee and M.G. Mendiratta, Abstract, J. of Metals, V. 33 (12), p. 6 (1981).
6. K. Aoki and D. Izumi, J. Japan Inst. Met., V. 43, p. 1190 (1979).
7. C.T. Liu, C.L. White and J.A. Horton, Acta Met., V. 33, p. 213 (1985).
8. A.I. Taub, S.C. Huang and K.M. Chang, Proc. Symp. on High Temperature Ordered Intermetallic Alloys, MRS, V. 39, Boston, p. 335 (1985).
9. H. Inoue, Proc. Symp. on High Temperature Ordered Intermetallic Alloys, MRS, V. 39, Boston, p. 255 (1985).
10. N.S. Stoloff in High Temperature Ordered Intermetallic Alloys, MRS Symposium, V. 39, C.C. Koch, C.T. Liu and N.S. Stoloff, Eds., Materials Res. Soc., Pittsburgh, PA, (1985) p. 3.
11. A.K. Kuruvilla, PhD Thesis, Rensselaer Polytechnic Institute, 1985.
12. S. Golwalker, PhD Thesis, Rensselaer Polytechnic Institute, 1984.
13. P.C. Paris and F. Erdogan, Trans ASME, J. Basic Eng., V. 85, p. 528 (1963).
14. N.S. Stoloff and R.G. Davies, Acta Met., V. 12, p. 473 (1964).
15. C.T. Liu, C.L. White and E.H. Lee, Scripta Met, V. 19, p. 1247 (1985).
16. A.K. Kuruvilla and N.S. Stoloff, Proc. 7th Int Conf on Strength of Metals and Alloys, Montreal, Canada, V. 2, p 1335, (1985).
17. E. Tschegg and S. Stanzl, Acta Met, V. 29, p. 33, (1981).
18. R.G. Davies and N.S. Stoloff, Trans TMS-AIME, V. 233, p. 714, (1965).
19. D.P. Pope and S.S. Ezz, Int. Met. Rev., V. 29, 1984, p. 136.
20. S. Takeuchi and E. Kuramoto, Acta Met, V. 21, p. 415 (1973).
21. M.H. Yoo, J.A. Horton and C.T. Liu, ORNL/TM-10709, Oak Ridge National Lab, July 1988.
22. V. Paidar, D.P. Pope and V. Vitek, Acta Met, V. 32, p. 435, (1984).
23. A.I. Taub, S.C. Huang and K.M. Chang, High Temperature Ordered Intermetallic Alloys, MRS Symposia, V. 39, p. 221, (1985).
24. K.H. Chien and E.A. Starke, Jr., Acta Met, V. 23, p. 1173, (1975).
25. N.R. Bonda, D.P. Pope and C. Laird, Acta Met, V. 35, p. 2371 (1987).
26. N.R. Bonda, D.P. Pope and C. Laird, Acta Met, V. 35, p. 2385, (1975).
27. J. Polak, Mat. Sci. and Eng., V. 92, p. 71 (1986).
28. P. Morgand, P. Mouturat and G. Sainfort, Acta Met, V. 16, p. 867 (1968).
29. J. Douin, P. Veyssieie and P. Beuchamp, Phil Mag A, V. 54, p. 375 (1986).
30. E. Hoffelner and M.O. Speidel, Creep and Corrosion, Cost-50 Second Round, CH-1 Final Reports, Brown-Boveri and Co., Baden, Switzerland, 1981.

TABLE 1

Alloy Compositions (at %) and Grain Sizes

Element	ORNL #1	ORNL #2	E361	E433	E434	E435
Fe	76.20	71.25	69.85	74.94	74.86	77.88
Al	23.71	28.67	28.35	24.93	25.05	21.88
Mn	----	----	1.735	0.027	0.029	0.030
Si	0.009	0.030	0.029	0.060	0.012	0.041
Ti	----	----	----	----	----	.120
Cu	----	----	----	0.008	0.008	0.011
Ni	----	----	0.006	0.003	0.002	0.003
Cr	----	----	0.002	0.003	0.003	0.004
Co	----	----	----	0.002	0.002	0.002
S	0.001	0.008	0.009	0.009	0.009	0.009
C	0.106	0.044	0.020	0.024	0.024	0.021
grain sizes μm	250	250	800	400	800	350

TABLE 2

Tensile Data for Alloys Tested

	σ_{ys} (MPa)	σ_{UTS} (MPa)	NSR*	Elong %	Ref
25°C					
Ni-24Al (HIP)	305	1345		34	
Ni-24Al (HIP + Extruded)	415	1520	0.56	34	
Ni-23.5Al-0.5Hf (wrought)	310	----	----	48	(20)
Ni-26Al (as cast)	290	490		6	
Ni-15Al-9.3Mn (HIP + extruded)	500	1000	1	24	
500°C					
Ni-24Al (HIP)	580	655		30	
Ni-24Al (HIP + Extruded)	1130	1255	0.92	36	
Ni-26Al (as cast)	---	580		0	
Ni-15Al-9.3Mn (HIP + extruded)	450	820	1	20	

*Notch Sensitivity Ratio = $\frac{(\sigma_{UTS})\ \text{notched}}{(\sigma_{UTS})\ \text{unnotched}}$

TABLE 3

Tensile Data for Fe-21.9%Al

DO_3 Order

Unnotched: σ_{ys} = 62 ksi
σ_{UTS} = 101 ksi
Ductility = 2-3%

Notched. σ_{UTS} = 58 ksi
Notch Sensitivity Ratio = 0.57

B2 Order

Unnotched: σ_{ys} = 80 ksi
σ_{UTS} = 104 ksi
Ductility = 2%

Notched: σ_{UTS} = 79 ksi
Notch Sensitivity Ratio = 0.79

TABLE 4

Slopes of Paris-Erdogan Equation

$da/dN = C\Delta K^m$

Fe-24.9%Al		m
B2 - RT	-	18
B2 - 600°C	-	2
DO_3 - RT	-	18
DO_3 - 500°C	-	4

T(°C)	%Al
25	DO_3
25	B2
500	DO_3
600	B2

TABLE 5

Dislocation Configurations after Fatigue Tests

(ORNL 1)	a% Al (E433)	(E434)	(ORNL 2)	(E361)
23.7	24.93	25.05	28.7	28.4
s*	s		p*	p
	s, p	p		
		p	p*	
		p, s		

p = dislocation pairs
s = single dislocations

TABLE 6

High Cycle Fatigue Data, $R \geq 0.1$

Alloy (at%)	T°C	Environment	$\Delta\sigma 10^6 / \sigma_{ys}$	$\Delta\sigma 10^7 / \sigma_{ys}$	Ref.
Fe-24Al-DO_3	25	Air	0.84	0.71	10
Fe-24Al-B2	25	Air	0.76	0.62	10
Fe-29Al-DO_3	25	Air	1.02	0.89	10
Fe-29Al-B2	25	Air	0.67	0.65	9
Ni-24Al HIP	25	Air	1.79	1.38	9
Ni-24Al HIP+Ext	25	Air	1.57	1.20	9
Ni-26Al Cast	25	Air	1.32	1.05	9
Ni_3Al (crystal)	25	Air	0.72	0.56	8
LRO-37 $(Fe,Ni)_3V$	25	Air	2.08	---	5
Nitac 14B	25	Air	1.25	1.12	32
MarM-200 (crystal)	25	Vac	0.55	0.47	8
Waspaloy	25	Air	0.57	0.48	35
IN617	25	Air	1.53	1.44	35
Hastelloy C	25	Air	---	1.05	35
Fe-24Al-DO_3	500	Air	1.08	0.83	10
Fe-29Al-DO_3	500	Air	1.01	0.83	10
Fe-24Al-B2	560	Air	0.68	---	10
Fe-29Al-B2	600	Air	0.95	---	10
Ni-24Al HIP+Ext	500	Air	0.98	0.92	9
Ni_3Al crystal	425	Air	0.42	0.33	8
Ni_3Al crystal	760	Air	0.36	0.28	8
LRO-1-3 $(Fe,Co,Ni)_3V$	650	argon	1.28	0.98	5
LRO-37 $(Fe,Ni)_3V$	400	argon	1.73	---	5
Nitac 14B	825	argon	1.30	1.11	32
U500	650	air	0.61	0.47	35
Waspaloy	800	air	0.50	0.46	35
IN718	650	air	0.56	0.44	35

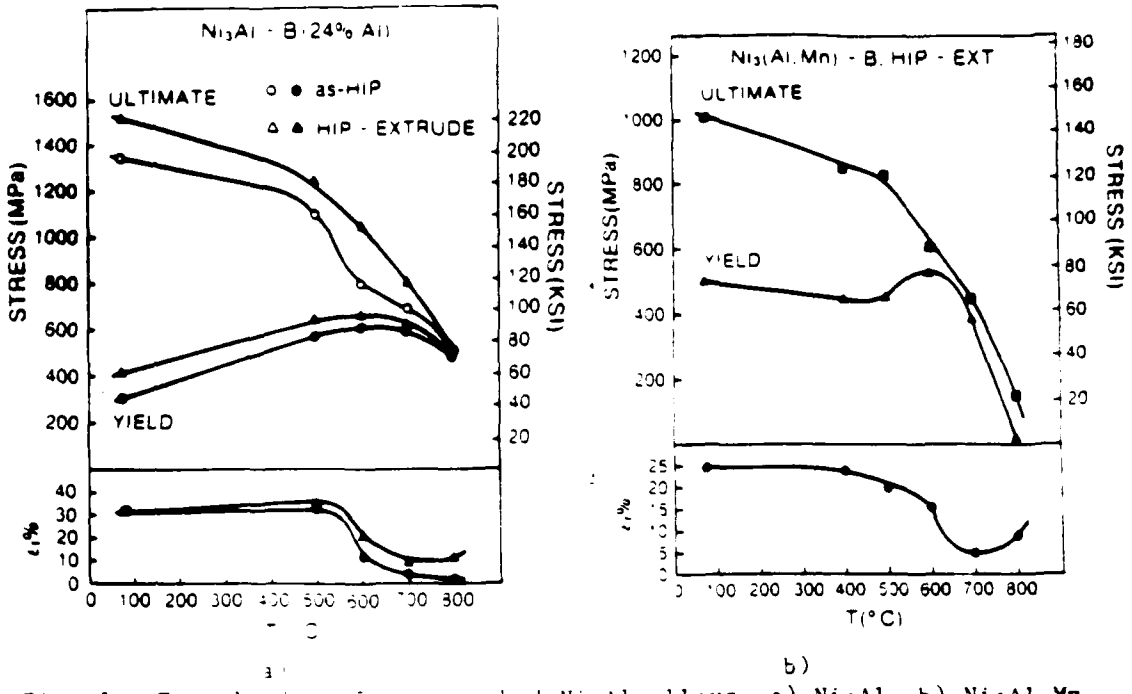

Fig. 1. Tensile data for unnotched Ni_3Al alloys a) Ni_3Al b) Ni_3Al,Mn

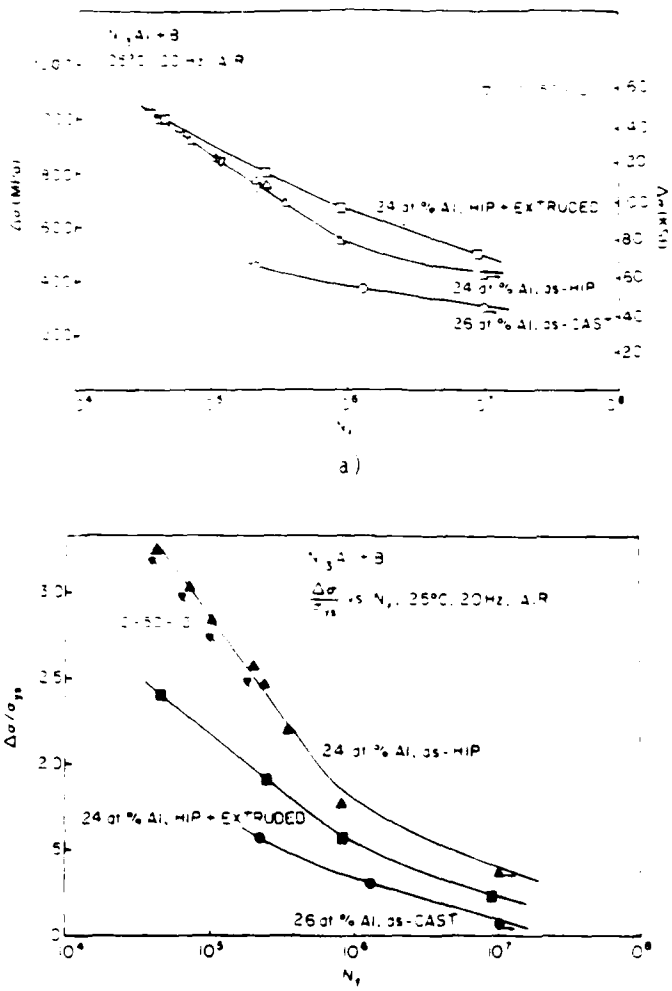

Fig. 2 High cycle fatigue of several Ni$_3$Al+B alloys [9]
a) σ-N data b) σ-N data normalized for differences in yield stress.

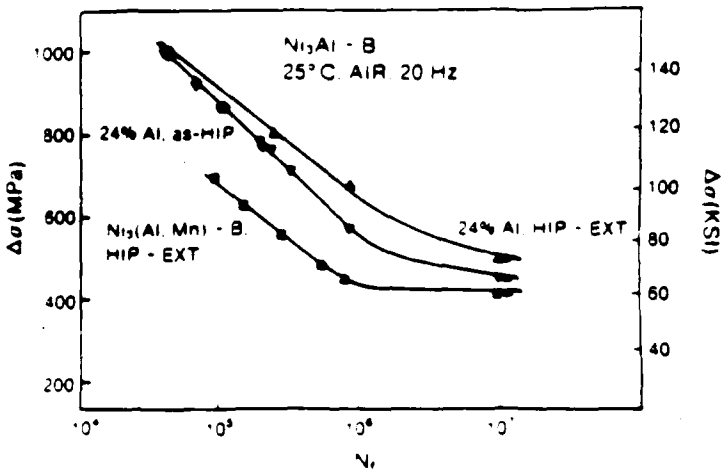

Fig. 3a) High cycle fatigue behavior at 25°C.

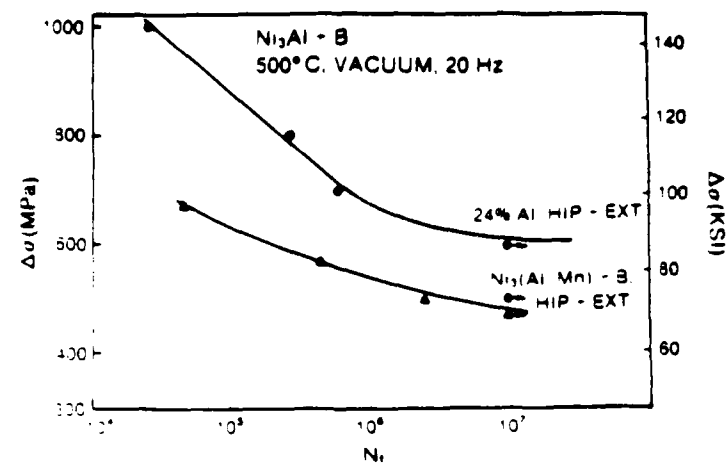

Fig. 3b) High cycle fatigue properties at 500°C.

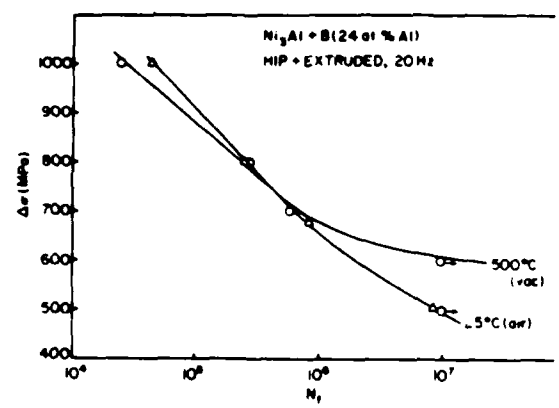

Fig. 4 Effect of temperature on high cycle fatigue behavior of HIP + extruded Ni-24a%Al+B.

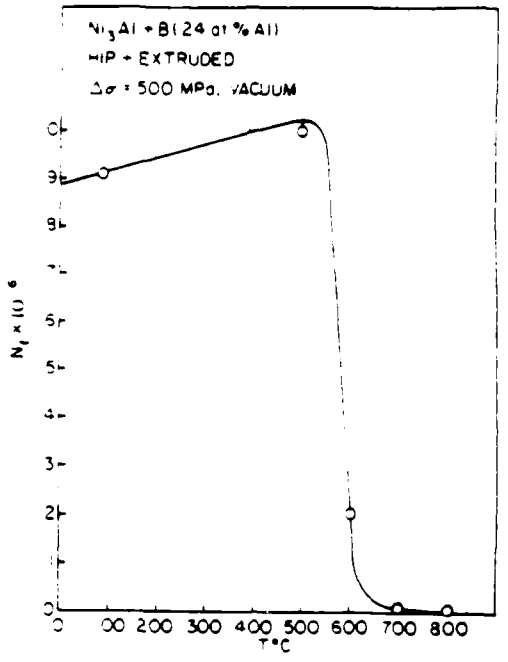

Fig. 5a) High cycle fatigue life vs temperature for Ni_3Al+B, $\Delta\sigma$=500MPa [9].

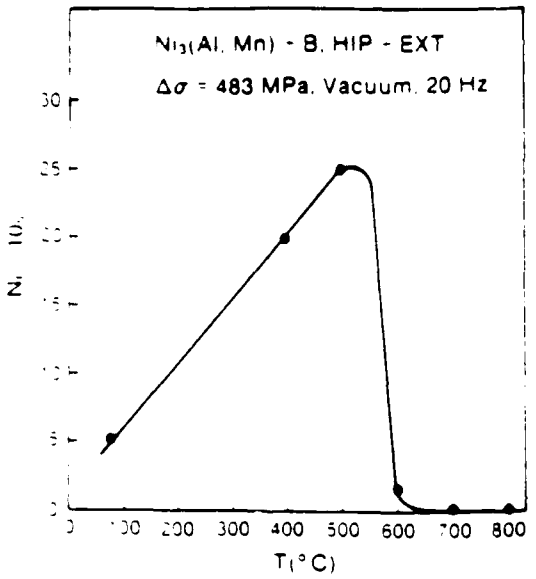

Fig. 5b) Effect of temperature on the HCF life of HIP+Ext $Ni_3(Al,Mn)$ at constant stress.

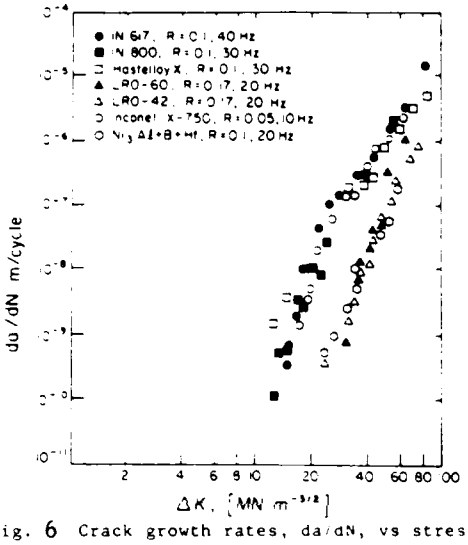

Fig. 6 Crack growth rates, da/dN, vs stress intensity factor range, ΔK, for IC-50, two LRO alloys[6] and several commercial alloys[5], room temperature, air.

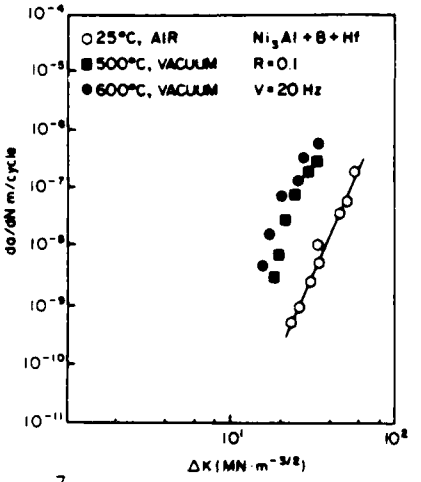

Fig. 7 Effect of temperature on crack growth of IC-50.

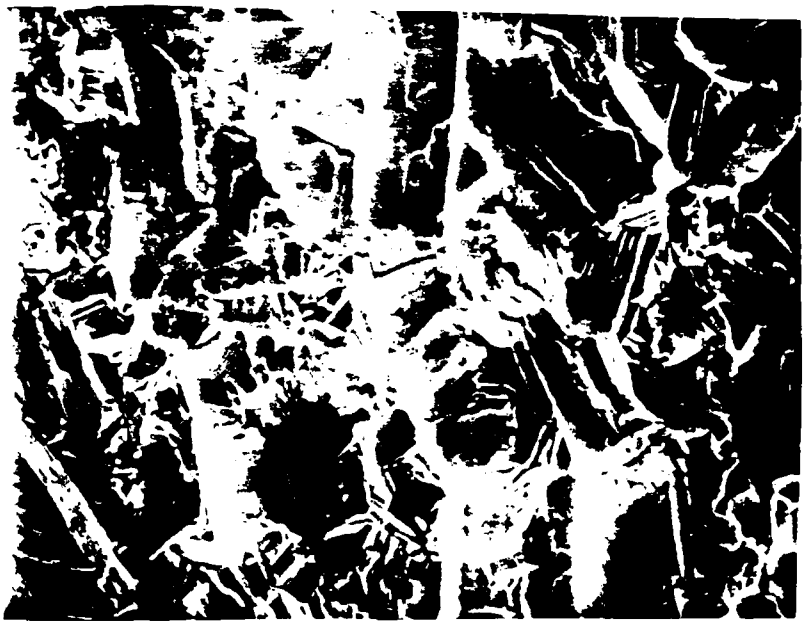

Fig. 8 Stage I (slip band) cracking in IC-50 cycled at 25 C.

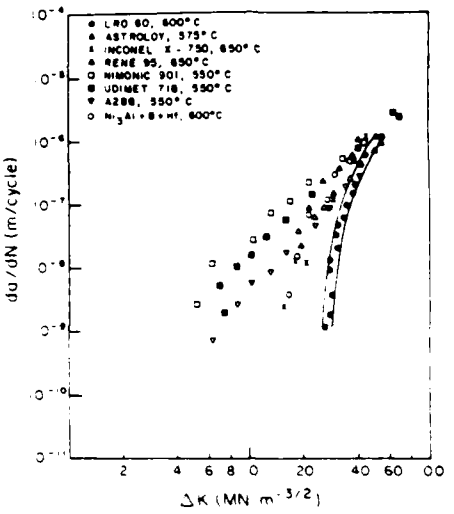

Fig. 9 Comparison of crack growth data for Ni_3Al and LRO-60[6] with other high temperature alloys. Astroloy tested in argon[7], R=0.05, ν=10Hz; Inconel X-750 tested in vacuum, R=0.05, ν=10Hz. René 95 tested in argon, R=0.05, ν=20Hz[7]. Nimonic 901, Udimet 718 and A-286 tested in air at R=0.1, ν=40 Hz[5], Ni_3Al+B+Hf tested in vacuum, R=0.01, ν=20 Hz.

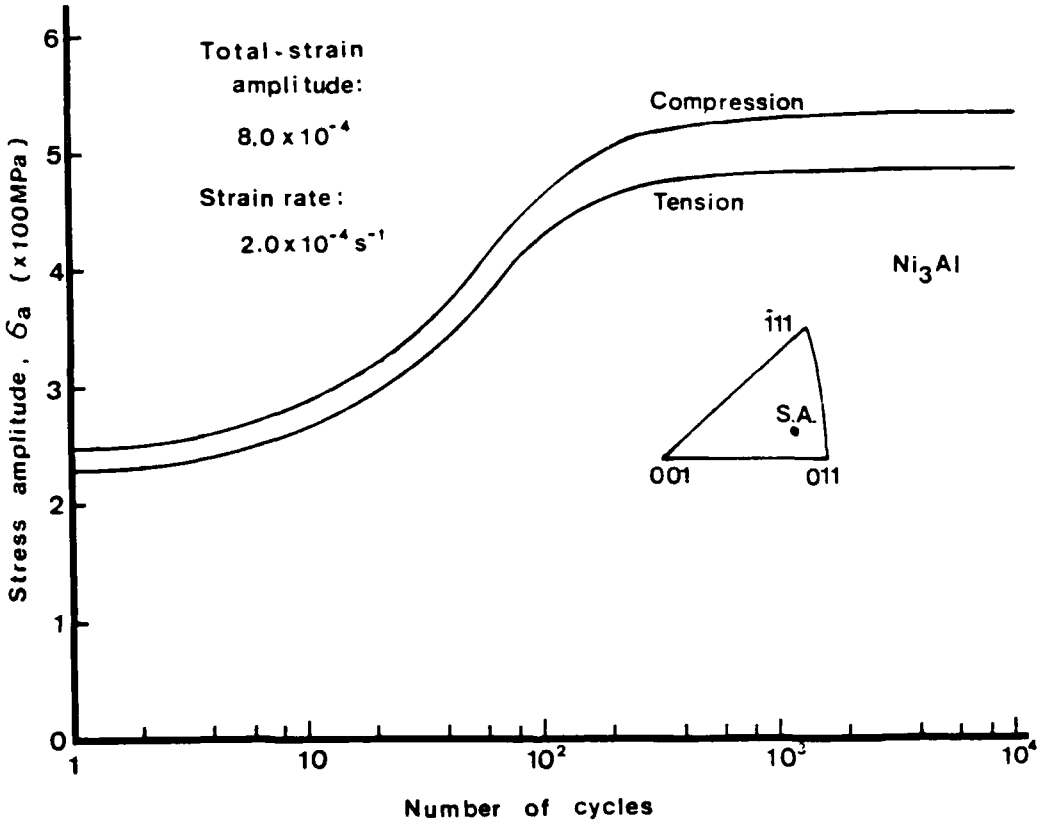

Fig. 10 Cyclic-hardening curve for the [$\bar{1}$ 10 13] oriented Ni_3Al+B single crystal cycled at $\Delta\varepsilon_t$=0.08%.

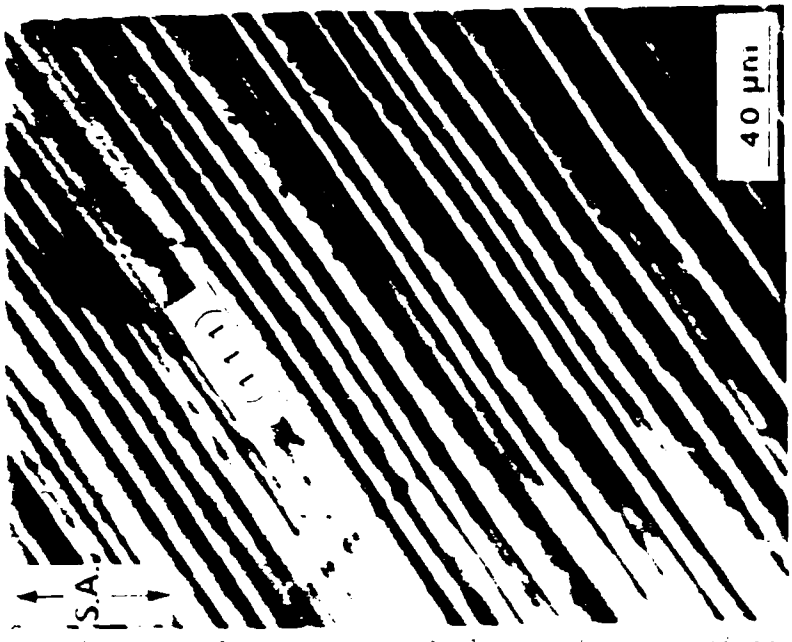

Fig. 11a) Optical micrograph of slip bands on specimen surface of the [1 10 13] oriented NiAl+B single crystal cycled at ε=0.15% after 50 cycles; surface roughening was observed.

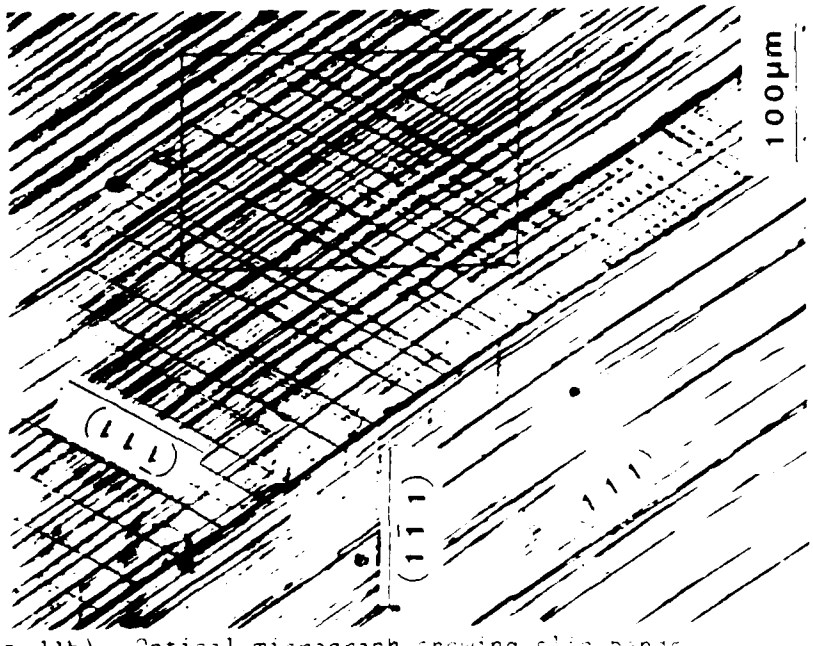

Fig. 11b) Optical micrograph showing slip bands associated with fatigue cracks on specimen surface of the same specimen in Fig. 11a. after 1,000 cycles.

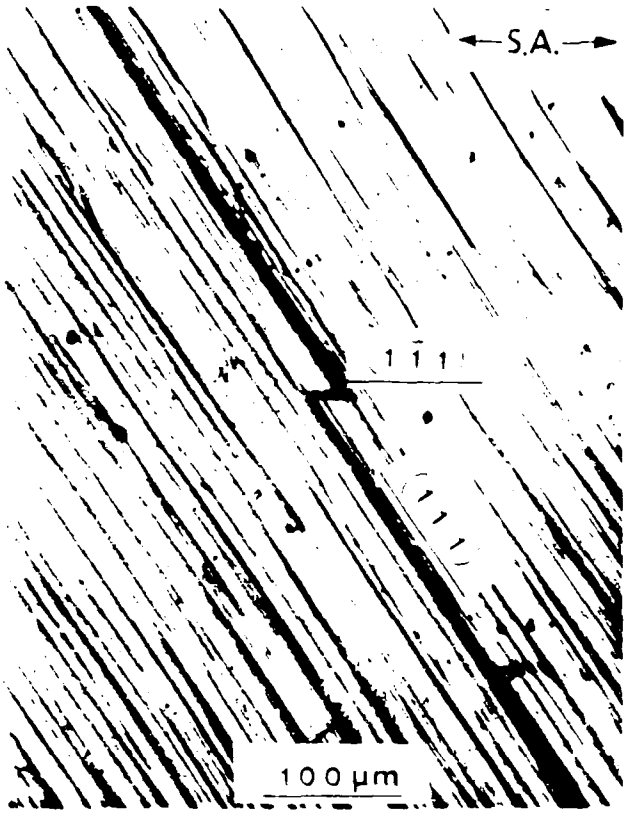

Fig. 12a [illegible] showing coplanar cracking [illegible] specimen surface of the specimen shown in Fig. 11

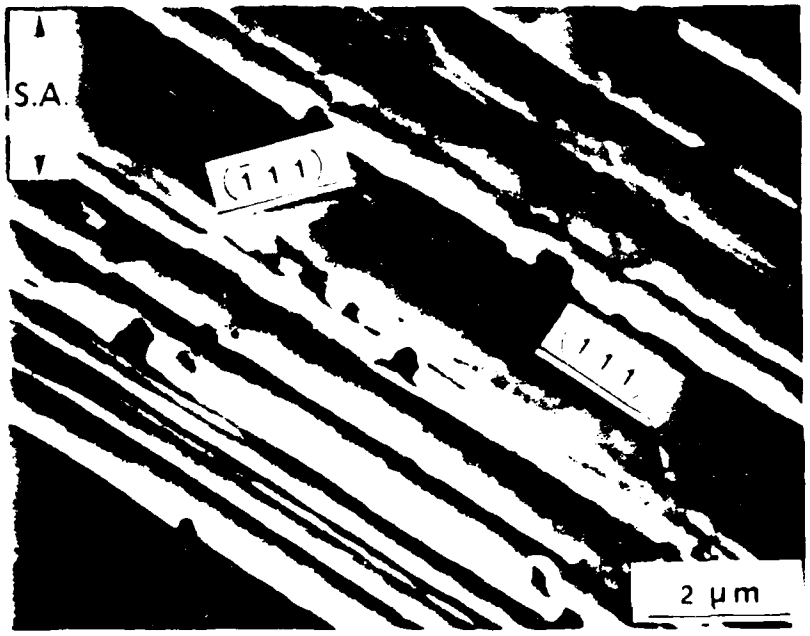

Fig. 12b [illegible] showing [illegible] slip bands at 4440 [illegible] specimen surface of [illegible] Fig. 11 [illegible] [illegible] [illegible] [illegible] at

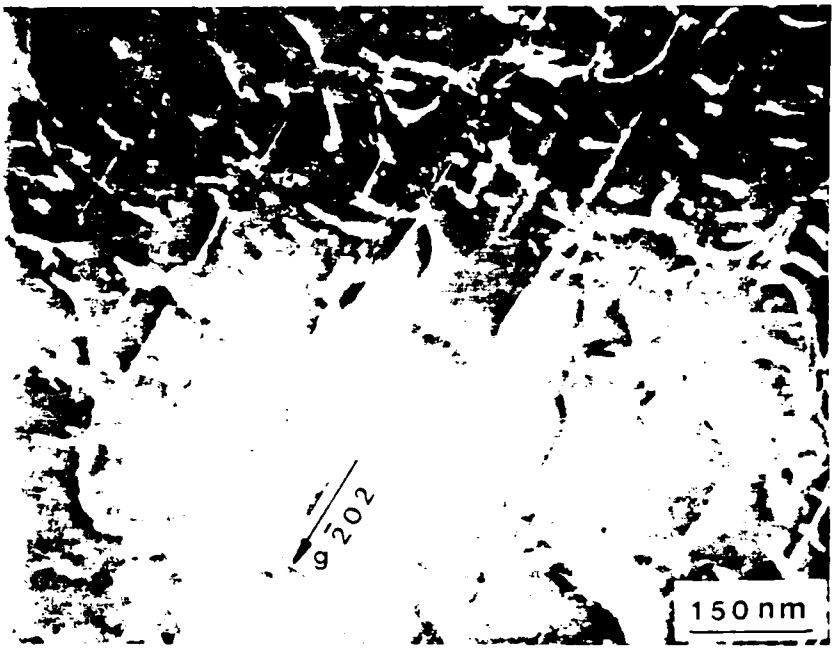

Fig. 13 Mutual annihilation of screw dislocations with opposite Burgers vectors; also large edge dipoles and small vacancy clusters; $\Delta\varepsilon$=0.16%, 44,900 cycles.

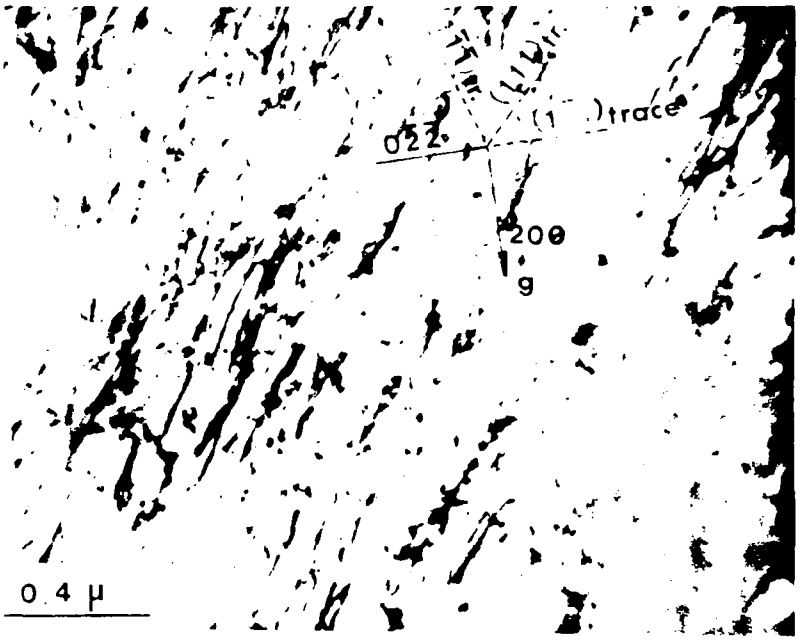

Fig. 14 Stacking fault tetrahedra suggesting vacancy condensation, $\Delta\varepsilon$=0.16%, 44,900 cycles.

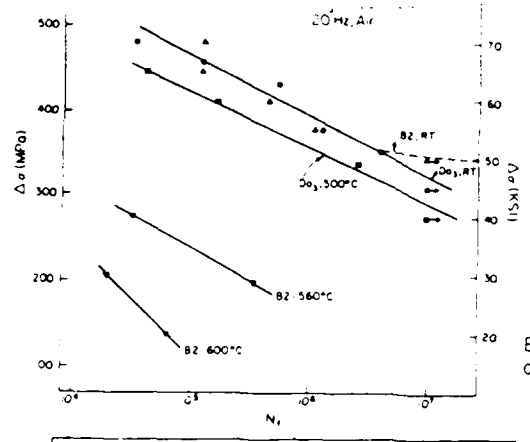

Fig. 15
Effects of temperature and type of order on HCF of Fe-23.7%Al

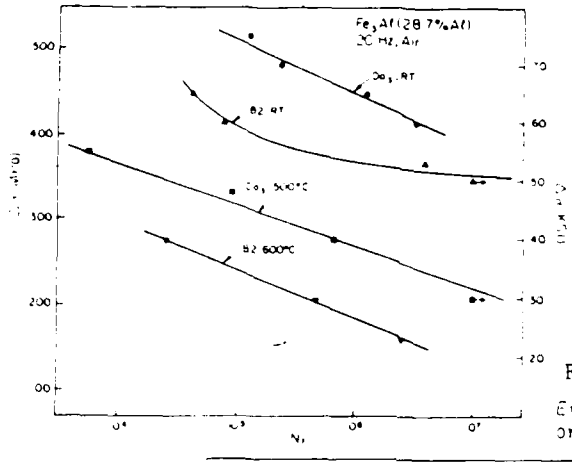

Fig. 16
Effects of temperature and type of order on HCF of Fe-28.7%Al

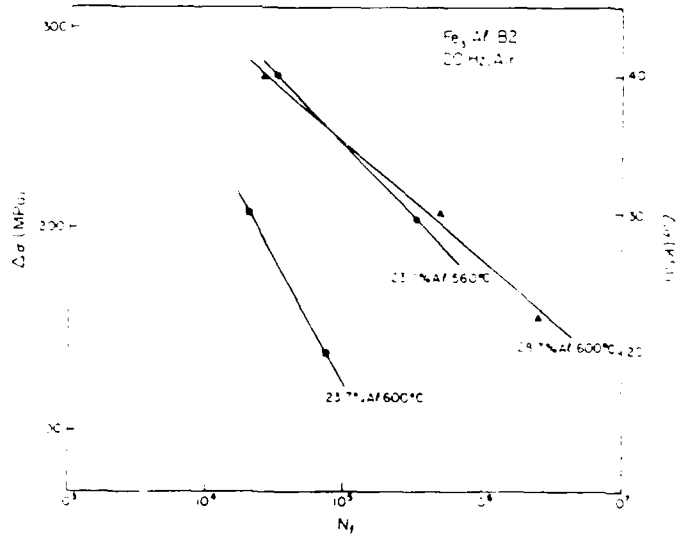

Fig. 17 Effect of temperature and composition on HCF of Fe_3Al in the B2 condition

initiation

b) mixed mode fatigue

Fig. 18 SEM fractographs of Fe-28.7%Al, HCF, 500°C

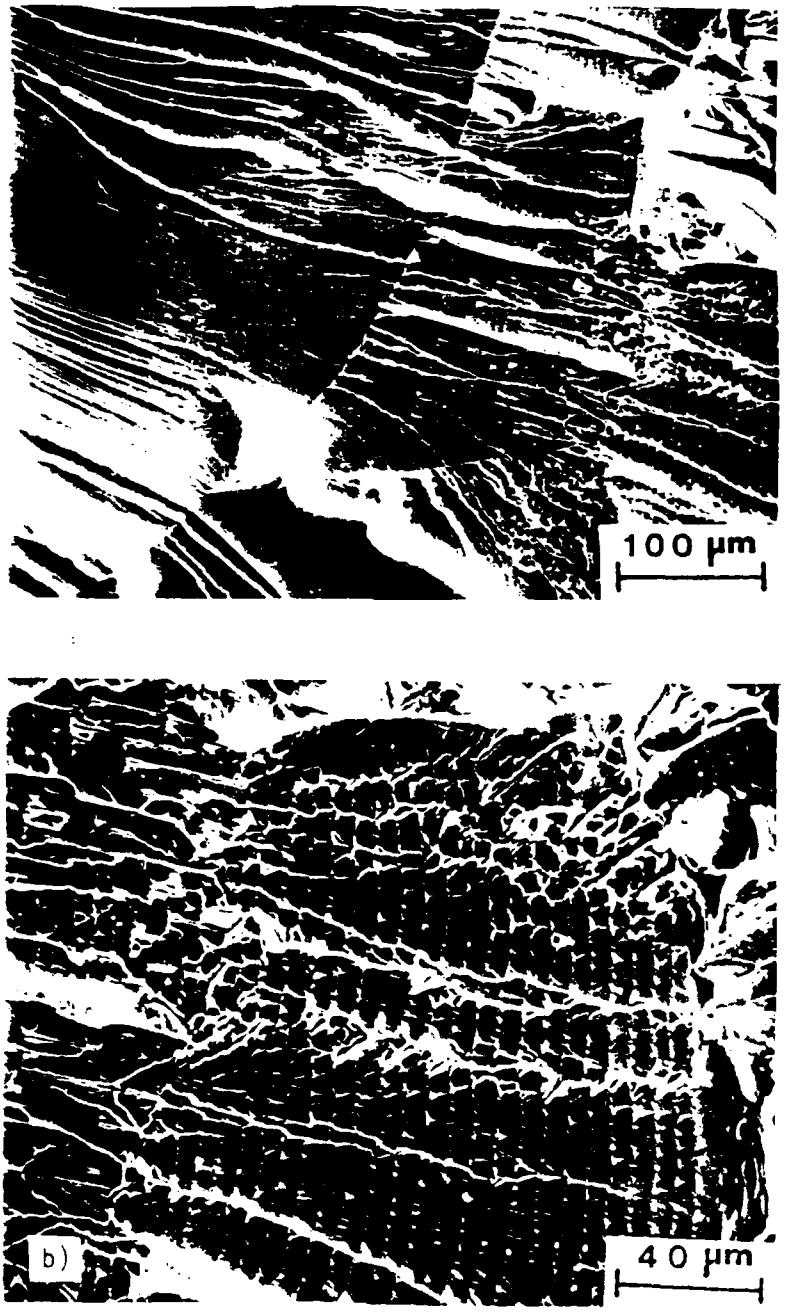

Fig. 19 Fatigue striations in Fe-28.7%Al, [illegible]

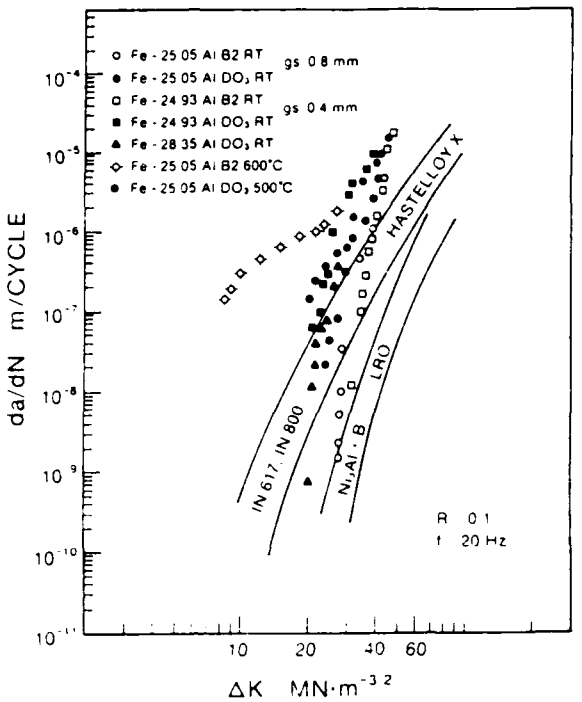

Fig. 20 Crack growth rates as a function of stress intensity factor. Data for LRO and Ni_3Al+B alloys from Ref. 11. Data for other alloys from Ref. 30.

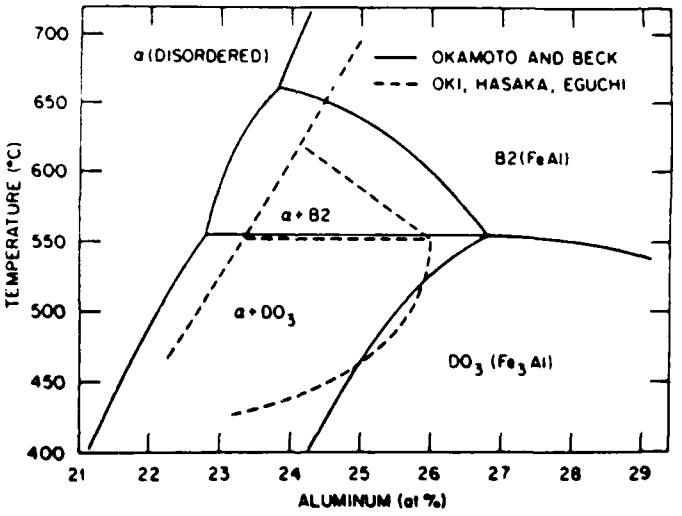

Fig. 21 Equilibrium and metastable Fe-Al system, from Ref. 9.

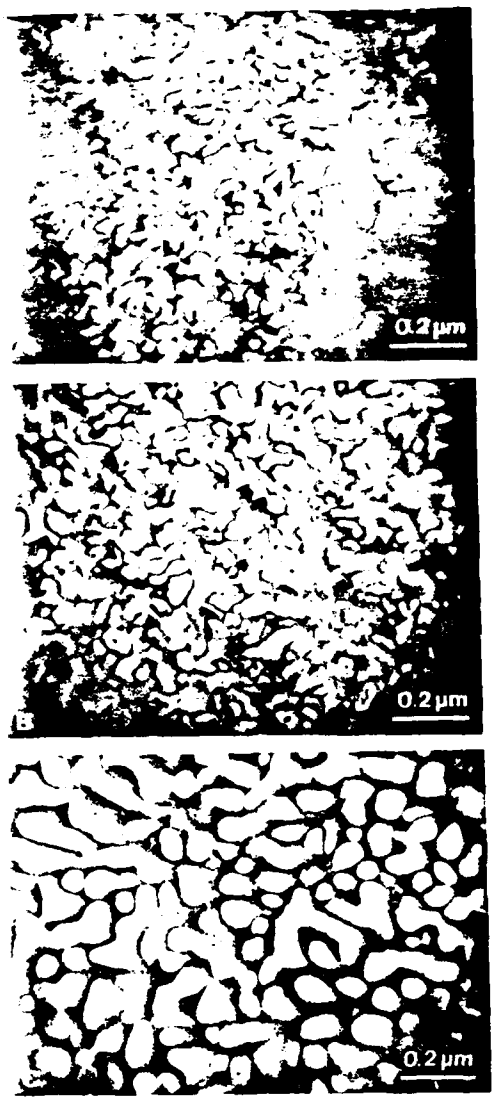

Fig. 22 α+DO$_3$ microstructures in fatigued Fe-23.7 at %Al for various test durations at 500°C; dark field TEM. (A) 30 min, N_f= 40,160, (B) 90 min, N_f = 162,000, (C) 36 h, N_f=2.645x10^6.

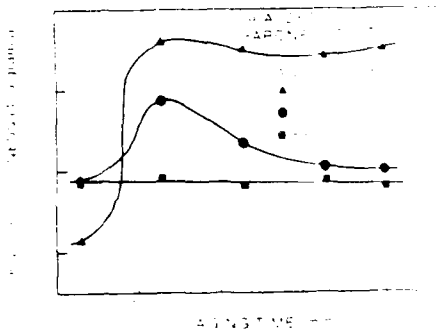

Fig. 23 Room temperature hardnes of fatigue specimens exposed for indicated times at each temperat

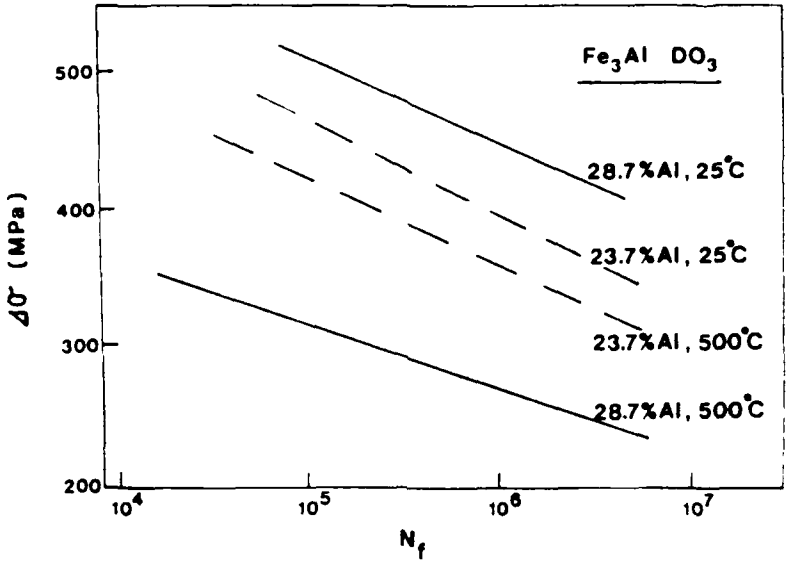

Fig. 24 Effects of temperature and composition on fatigue of Fe_3Al.